Check for updates

Paleoceanography and Paleoclimatology

RESEARCH ARTICLE
10.1029/2023PA004650

Special Section:
Illuminating a Warmer World: Insights from the Paleogene

Key Points:

- Benthic foraminiferal clumped isotope thermometry is used to reconstruct deep-sea temperatures at the Eocene-Oligocene Transition
- The onset of large-scale Antarctic glaciation is associated with an abrupt ~5°C cooling of the deep eastern equatorial Pacific Ocean
- This cooling is short-lived suggesting Antarctic glaciation did not have a long-term impact on deep-sea temperatures in the Pacific Ocean

Supporting Information:

Supporting Information may be found in the online version of this article.

Correspondence to:

V. E. Taylor,
victoria.taylor@uib.no

Citation:

Taylor, V. E., Wilson, P. A., Bohaty, S. M., & Meckler, A. N. (2023). Transient deep ocean cooling in the eastern equatorial Pacific Ocean at the Eocene-Oligocene Transition. *Paleoceanography and Paleoclimatology*, *38*, e2023PA004650. https://doi.org/10.1029/2023PA004650

Received 30 MAR 2023
Accepted 26 JUL 2023

© 2023. The Authors.
This is an open access article under the terms of the Creative Commons Attribution License, which permits use, distribution and reproduction in any medium, provided the original work is properly cited.

Transient Deep Ocean Cooling in the Eastern Equatorial Pacific Ocean at the Eocene-Oligocene Transition

V. E. Taylor[1,2], P. A. Wilson[2], S. M. Bohaty[2,3], and A. N. Meckler[1]

[1]Department of Earth Science, Bjerknes Centre for Climate Research, University of Bergen, Bergen, Norway, [2]National Oceanography Centre, School of Ocean and Earth Science, University of Southampton, Southampton, UK, [3]Now at Institute of Earth Science, Heidelberg University, Heidelberg, Germany

Abstract At the Eocene-Oligocene Transition (EOT), approximately 34 million years ago, Earth abruptly transitioned to a climate state sufficiently cool for Antarctica to sustain large ice sheets for the first time in tens to hundreds of millions of years. Oxygen isotope records from deep-sea benthic foraminifera ($\delta^{18}O_b$) provide the foundation of our understanding of this pivot point in Cenozoic climate history. A deeper insight, however, is hindered by the paucity of independent deep-sea temperature reconstructions and the ongoing challenge of deconvolving the temperature and continental ice volume signals embedded in $\delta^{18}O_b$ records. Here we present records of deep-sea temperature change from the eastern equatorial Pacific for the EOT using clumped isotope thermometry, which permits explicit temperature reconstructions independent of seawater chemistry and continental ice volume. Our records suggest that the deep Pacific Ocean cooled markedly at the EOT by 4.7 ± 0.9°C. This decrease in temperature represents the first direct and robust evidence of deep-sea cooling associated with the inception of major Cenozoic glaciation. However, our data also indicate that this major cooling of the deep Pacific Ocean at the EOT was short-lived (~200 kyrs), with temperatures rebounding to values close to pre-EOT levels by 33.6 Ma. Our calculated record of seawater $\delta^{18}O$ suggests that this rebound in ocean temperature occurred despite the continued presence of a large-scale Antarctic ice sheet. This finding suggests a degree of decoupling between deep ocean temperatures in the eastern equatorial Pacific Ocean and the behavior of the newly established Antarctic ice sheet.

1. Introduction

The abrupt onset of sustained large-scale Antarctic glaciation approximately 34 million years ago, at the Eocene-Oligocene Transition (EOT), was a pivot point in Cenozoic climate history (Coxall et al., 2005; Zachos et al., 1992, 1996) because it signaled the rise of a new unipolar glacial climate state (Spray et al., 2019). The introduction of Antarctic ice sheets into the Earth system fundamentally changed the predictability of Earth's climate response to astronomical forcing (Westerhold et al., 2020). Long term decline in atmospheric carbon dioxide concentrations, in the context of an astronomical configuration conducive to cool austral summers, is suggested to have triggered the onset of sustained large-scale Antarctic glaciation (Coxall et al., 2005; DeConto & Pollard, 2003). Our understanding of the EOT currently relies heavily on records of stable oxygen isotope data ($\delta^{18}O$) from deep-sea benthic foraminifera ($\delta^{18}O_b$). These records indicate a 1.2–1.5‰ increase at the EOT (Zachos et al., 1996) across two main steps or phases (Coxall et al., 2005). An initial, up to ~0.5‰ increase was inferred to be rapid for "Step 1" (Coxall & Wilson, 2011; Coxall et al., 2005) and dated to ~34.15 Ma (Pearson et al., 2008). This initial $\delta^{18}O_b$ increase, however, is not rapid or step-like in form in a stratigraphically more complete section from the eastern equatorial Pacific Ocean (Taylor et al., 2023b). A rapid globally synchronous $\delta^{18}O_b$ increase of at least 0.9‰ is documented for "Step 2" and dated to ~33.65 Ma (Coxall & Wilson, 2011; Coxall et al., 2005). This $\delta^{18}O_b$ increase has been referred to as the EOIS (~33.65 Ma; Hutchinson et al., 2021). A transient "overshoot" in $\delta^{18}O_b$ is observed immediately following the EOIS (Zachos et al., 1996) and deep-sea $\delta^{18}O_b$ values remain high for ~500 kyrs during the earliest Oligocene glacial maximum (EOGM; ~33.65 to ~33.16 Ma after Liu et al., 2004). Yet, while both the overall amplitude and structure of the $\delta^{18}O_b$ change across the EOT are now reasonably well established (Coxall & Wilson, 2011; Coxall et al., 2005; Langton et al., 2016; Pusz et al., 2011; Taylor et al., 2023b; Zachos et al., 1996), the drivers of the $\delta^{18}O_b$ increase are not. A main problem limiting progress is the unresolved attribution of the $\delta^{18}O_b$ signal because it is sensitive to changes in both ocean temperature and seawater $\delta^{18}O$ ($\delta^{18}O_{sw}$), with the latter influenced globally, by changes in continental ice volume and, regionally, by salinity.

In early studies the overall increase in $\delta^{18}O_b$ from the late Eocene to early Oligocene was attributed entirely to temperature change, equating to at least 4–6°C of deep-sea cooling (Kennett & Shackleton, 1976; Savin, 1977; Savin et al., 1975; Shackleton & Kennett, 1975). Subsequent analysis of Southern Ocean drill cores revealed an abrupt appearance of ice-rafted debris (IRD) and chemically immature clay minerals (e.g., Ehrmann & Mackensen, 1992; Hambrey et al., 1991; Zachos et al., 1992) coincident with "Step 2" (Scher et al., 2011). These findings indicated that a component of the observed $\delta^{18}O_b$ increase must instead be attributed to an increase in $\delta^{18}O_{sw}$ driven by the initiation of large Antarctic ice sheets. Sequence stratigraphic records of sea level fall have also been used to attribute an ice volume contribution to the $\delta^{18}O_b$ increase (Houben et al., 2012; Miller et al., 2008, 2020; Pekar et al., 2002). These records, however, lack sufficient age control and temporal resolution to help tease apart the evolution of deep-sea temperatures and continental ice volume across the EOT. Independent temperature reconstructions are, therefore, needed to discriminate between the temperature and $\delta^{18}O_{sw}$ components of $\delta^{18}O_b$ records.

One approach to deconvolving deep-sea $\delta^{18}O_b$ for temperature and $\delta^{18}O_{sw}$ is to develop surface ocean temperature records from high latitude regions proximal to sites of deep convection (e.g., Bohaty et al., 2012; Liu et al., 2009; Petersen & Schrag, 2015). The premise of this approach relies on temperature signals in these regions being translated to the deep ocean. Spatial heterogeneity and temporal variability in surface ocean cooling during the EOT, however, complicate the use of sea surface temperatures (SSTs) to deconvolve $\delta^{18}O_b$ (e.g., Bohaty et al., 2012; Houben et al., 2019; Lear et al., 2008; Liu et al., 2009, 2018; Petersen & Schrag, 2015; Plancq et al., 2014; Tremblin et al., 2016; Wade et al., 2012; Śliwińska et al., 2019). A more direct approach to deconvolving $\delta^{18}O_b$ into its two component parts is to apply the Mg/Ca paleothermometer to benthic foraminifera across the EOT (e.g., Billups & Schrag, 2003; Coxall et al., 2018; Katz et al., 2008; Lear et al., 2000, 2004, 2008, 2010; Pusz et al., 2011). Records from shallow low latitude continental shelf sites identify ~2°C to ~4°C of cooling associated with "Step 1" and negligible cooling across the EOIS. Based on these records it has been suggested that the "Step 1" $\delta^{18}O_b$ increase was driven predominantly by cooling and the subsequent EOIS $\delta^{18}O_b$ increase by Antarctic glaciation, with only a minor temperature component. The extent to which these benthic foraminiferal Mg/Ca records from continental shelf sites are representative of deep-ocean temperature change, however, remains unclear. This is because many deep-sea Mg/Ca records fail to detect any cooling across the EOT (e.g., Billups & Schrag, 2003; Lear et al., 2000, 2004; Pusz et al., 2011). The absence of cooling in deep-sea Mg/Ca records is attributed to competing secondary, non-thermal influences on benthic foraminiferal Mg/Ca records (Lear et al., 2004, 2010; Peck et al., 2010; Pusz et al., 2011). The most problematic of these non-thermal influences for the EOT is the increase in carbonate ion concentration (Lear et al., 2004) associated with the rapid deepening of the calcite compensation depth (CCD) (Coxall et al., 2005). This acts to increase benthic foraminiferal Mg/Ca ratios, obscuring deep-sea cooling signals (Elderfield et al., 2006; Lear et al., 2010; Yu & Elderfield, 2008). Despite attempts to use Li/Ca to correct for the carbonate ion effect this problem persists (Lear et al., 2010; Peck et al., 2010; Pusz et al., 2011) and must be acute in the earliest Oligocene because the CCD over-deepens markedly (Taylor et al., 2023b). As a result, there are currently no robust records of deep-sea temperature change across the EOIS or EOGM.

Here we present multiply substituted "clumped" isotope (Δ_{47}) bottom-water temperature (BWT) records from the deep eastern equatorial Pacific (EEP; Integrated Ocean Drilling Program (IODP) Expedition 320 Sites U1334 and U1333, and ODP Leg 199 Site 1218). Exploiting the temperature dependence of bonding between two heavy isotopes (^{13}C and ^{18}O) within carbonate ions (Ghosh et al., 2006; Schauble et al., 2006), the carbonate clumped isotope thermometer is independent of the isotopic composition of the seawater from which the calcium carbonate precipitated (Eiler, 2011). Furthermore, it is suggested to be unaffected by influences other than ocean temperature, including foraminiferal species-specific vital effects (Grauel et al., 2013; Meinicke et al., 2020; Peral et al., 2018; Piasecki et al., 2019; Tripati et al., 2010), seawater pH and salinity (Tripati et al., 2015; Watkins & Hunt, 2015), and, crucially for the EOT, changes in calcium carbonate saturation state (Eagle et al., 2013; Hill et al., 2014). Analytical uncertainty, however, is inherently large and considerable sample amounts are required to achieve the levels of analytical precision needed to tackle palaeoclimate questions. Recent advances in analytical techniques have reduced the required sample size and enabled a multiple replicate analysis approach for deriving clumped isotope temperatures (e.g., Hu et al., 2014; Meckler et al., 2014; Müller et al., 2017; Schmid & Bernasconi, 2010), broadening the scope of applicability of the clumped isotope thermometer to foraminifera (e.g., Evans et al., 2018; Leutert et al., 2020, 2021; Modestou et al., 2020; Rodríguez-Sanz et al., 2017). For a multiple replicate analysis approach, measurements can either be sourced from one larger sample (as in Meckler

25724525, 2023, 8, Downloaded from https://agupubs.onlinelibrary.wiley.com/doi/10.1029/2023PA004650 by University Of Southampton, Wiley Online Library on [09/10/2023]. See the Terms and Conditions (https://onlinelibrary.wiley.com/terms-and-conditions) on Wiley Online Library for rules of use; OA articles are governed by the applicable Creative Commons License

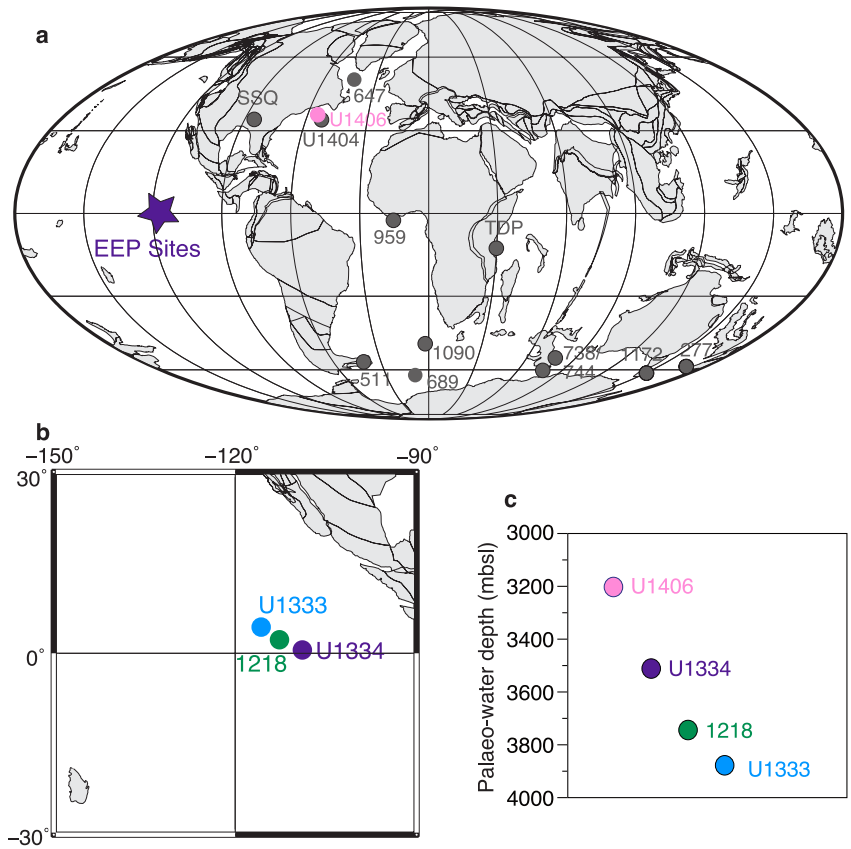

Figure 1. Location of sites studied. (a) Palaeo-locations of study sites and sites referred to within the text. Sites are shown in their palaeo-locations at 34 Ma (numbers refer to Deep Sea Drilling Project and Integrated Ocean Drilling Program sites (now International Ocean Discovery Program)); SSQ = St Stephen's Quarry; TDP = Tanzania Drilling Project) and maps (palaeogeographic reconstruction for 34 Ma) were generated using http://www.odsn.de. (b) Detailed view of study site region in the EEP. Palaeo-locations of sites in the eastern equatorial Pacific (EEP) taken from Pälike et al. (2012) and calculated using Koppers et al. (2001). (c) Shows palaeo-water depth estimates for the study sites and one other main deep ocean site at 34 Ma. Palaeo-water depth estimates at 34 Ma for sites in the EEP are taken from Pälike et al. (2012), and for Site U1406 are taken from Norris et al. (2014). Palaeo-locations of our study sites are listed in Table S1 in Supporting Information S1.

et al., 2022) or by combining individual monospecific measurements from multiple closely spaced samples (this study). One example of the success of the multiple replicate analysis approach is a benthic foraminiferal Δ_{47} BWT record from the North Atlantic Ocean, spanning the Cenozoic, which suggests a long-term 5–6°C cooling occurred between the late Eocene to early Oligocene (Meckler et al., 2022). However, that record requires testing in other ocean basins and is of insufficient resolution to study the relationship between changes in $\delta^{18}O_b$, BWT, and $\delta^{18}O_{sw}$ at the EOT. Our new data from the deep EEP provide the first direct and independent documentation of BWT change associated with the initiation of sustained large-scale Antarctic glaciation.

2. Materials and Methods

2.1. Study Sites

IODP Expedition 320 Sites U1334 (7°59.998′N, 131°58.408′W) and U1333 (10°30.996′N, 138°25.159′W) (Pälike et al., 2010), and Ocean Drilling Program (ODP) Leg 199 Site 1218 (8°53.378′N, 135°22.000′W) (Lyle et al., 2002) are located in the EEP Ocean (Figure 1). These sites are well located to record a signal representative of global change because the Pacific Ocean was even larger during the Paleogene than it is today and therefore accounts for a significant proportion of the global deep ocean (Lyle et al., 2002, 2008; Pälike et al., 2010). The seminal benthic foraminiferal stable isotope stratigraphy for the EOT comes from Site 1218 (Coxall & Wilson, 2011; Coxall et al., 2005). That record, however, suffers from a ∼300 kyr-long condensed interval of non-carbonate burial at the base of the EOT. However, a more stratigraphically complete record for this interval

25724525, 2023, 8, Downloaded from https://agupubs.onlinelibrary.wiley.com/doi/10.1029/2023PA004650 by University Of Southampton, Wiley Online Library on [09/10/2023]. See the Terms and Conditions (https://onlinelibrary.wiley.com/terms-and-conditions) on Wiley Online Library for rules of use; OA articles are governed by the applicable Creative Commons License

is now available from nearby Site U1334 (Figure 1) which benefits from higher carbonate contents because of its shallower paleowater depth (Taylor et al., 2023b). The benthic foraminiferal stable isotope stratigraphy from Site U1334 is broadly consistent with the record from Site 1218 with two notable exceptions. First, the $\delta^{18}O_b$ increase across "Step 1" is not rapid nor step-like in structure and, second, a pronounced transient negative carbon isotope excursion (nCIE) occurs correlative to the condensed carbonate-free interval at Site 1218 (Taylor et al., 2023b). Herein we use the $\delta^{18}O_b$ stratigraphy for the EOT from Site U1334 (Taylor et al., 2023b; Figure S1 in Supporting Information S1). We followed the splice, depth-scale revisions, and site-to-site correlations of Westerhold et al. (2012). All of our EEP records are shown on a common astronomically calibrated age model, based on the tuning of X-ray fluorescence (XRF) core scanning Si, Fe, and Ca records to the stable long eccentricity cycle (Westerhold et al., 2014).

2.2. Sample Processing

At all sites, 2 cm-thick quarter-round scoop samples (~30 cc) were oven dried at 50°C, soaked in buffered 0.2% sodium hexametaphosphate, and washed over 63 μm sieves using de-ionized (DI) water. The >63 μm residue was oven dried overnight at 50°C. All *Cibicidoides* spp. specimens were picked from the 250–500 μm size fraction and sorted into monospecific aliquots. At Sites U1334 and 1218, *Oridorsalis umbonatus* specimens were also picked from the 250–500 μm size fraction. Individual specimens were gently cracked open between glass slides. Fragments were ultra-sonically cleaned in methanol twice, and DI water once, and rinsed in DI water three times to remove adhering clays and infilling. An additional methanol sonication, and two DI water rinses, were required for specimens from Site 1218 to ensure all adhering clays and infilling were removed. All cleaned fragments were oven dried overnight at 50°C. Benthic foraminiferal specimens at all our sites show good to moderate preservation and are suggested to robustly record $\delta^{13}C_b$ and $\delta^{18}O_b$ values (Edgar et al., 2013). Diagenetic overprinting has a negligible impact on measured benthic foraminiferal Δ_{47} values in typical deep ocean settings (Leutert et al., 2019).

2.3. Multiply Substituted "Clumped" Isotope Thermometry

Carbonate clumped isotope analysis was conducted at the University of Bergen (UiB) using two Thermo Fisher Scientific Kiel IV carbonate preparation devices coupled to MAT-253 Plus isotope ratio mass spectrometers. All measurements were generated following the method described in detail by Meinicke et al. (2020). In summary, sample and powdered carbonate standard aliquots (85–105 μg) were individually reacted at 70°C with ~104% phosphoric acid. Organic contaminants and sulfide components were removed from the evolved CO_2 gas using a Porapak-QTM (ethylvinylbenzene and divinylbenzene copolymer bead) trap and silver-wool, respectively, held within a sulfinert coated stainless steel tube kept at −20°C. For cleaning purposes, once a day, the Porapak-QTM trap was baked at 120°C for at least 1 hr. Sample and reference gas were analyzed for 400 s each using the long-integration dual-inlet (LIDI) method (Hu et al., 2014; Müller et al., 2017). Masses 44–49 were collected for both sample and reference gas to determine Δ_{47}, $\delta^{13}C$, and $\delta^{18}O$ values (masses 44–47) and to monitor potential contaminants (masses 48–49). Daily peak scans were used to correct all measurements for pressure-dependent baseline (PBL) effects (Bernasconi et al., 2013; Meckler et al., 2014). Powdered carbonate standards (ETH 1–4; Bernasconi et al., 2018, 2021) were used to monitor instrument performance (ETH 4) and standardize and transfer Δ_{47} values (ETH 1–3) to the I-CDES scale (Bernasconi et al., 2021). Carbonate standards ETH 1–3 were used to correct $\delta^{13}C$ and $\delta^{18}O$ for instrument drift and for scale compression. Sample and carbonate standard aliquots were measured in a roughly 1:1 ratio, with the number of measurements of each of the carbonate standard per run selected to maximize accuracy and precision of the empirical transfer function (ETF; Kocken et al., 2019). We used the IUPAC ^{17}O correction parameters (Brand et al., 2010; Daëron et al., 2016) and all raw data processing was performed using the Easotope software package (John & Bowen, 2016).

No inter-species offsets in benthic foraminiferal Δ_{47} values have been observed, enabling us to combine individual monospecific measurements from different species (Modestou et al., 2020; Piasecki et al., 2019) to calculate an average Δ_{47} value. Precision of individual temperatures is maximized by averaging across a minimum of 30 measurements of aliquots of monospecific benthic foraminifera sourced from multiple (n = 11–34) closely spaced samples. Precision of baseline temperatures is further maximized by combining a greater number (n = 69–251) of individual measurements across longer stratigraphic intervals and from all three sites (see Tables S2–S4 in Supporting Information S1). Temperatures were calculated from corrected mean Δ_{47} values using the

25724525, 2023, 8, Downloaded from https://agupubs.onlinelibrary.wiley.com/doi/10.1029/2023PA004650 by University Of Southampton, Wiley Online Library on [09/10/2023]. See the Terms and Conditions (https://onlinelibrary.wiley.com/terms-and-conditions) on Wiley Online Library for rules of use; OA articles are governed by the applicable Creative Commons License

10.1029/2023PA004650

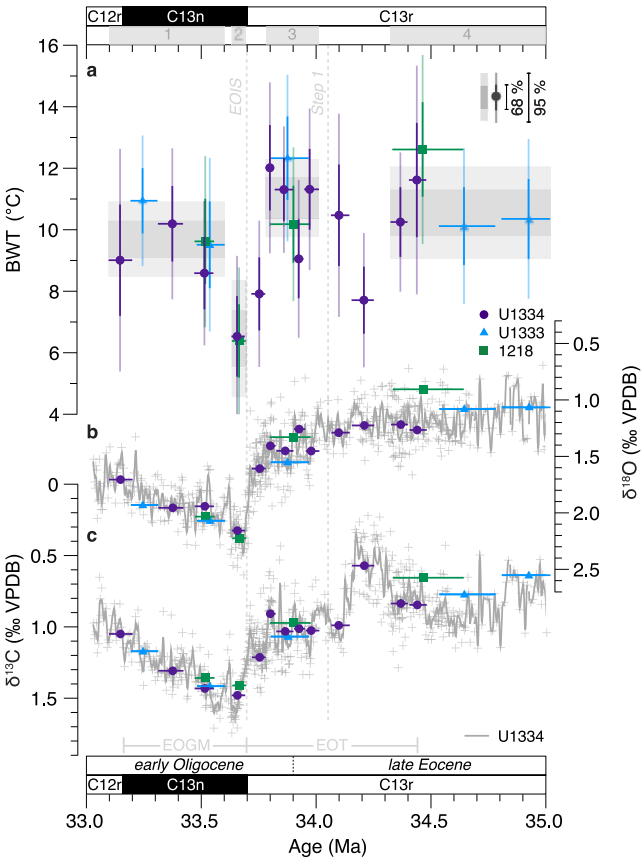

Figure 2. Bottom-water temperature reconstructions from the eastern equatorial Pacific. Panel (a) shows Δ_{47}-derived bottom-water temperatures for Site U1334 (circles), 1218 (squares), and U1333 (triangles). Horizontal bars represent the stratigraphic range from which measurements are pooled and are smallest for Site U1334 due to higher sedimentation rates and benthic foraminiferal abundance relative to Sites U1333 and 1218. *Y*-axis error bars represent 68% and 95% confidence intervals considering both analytical and calibration uncertainty. Gray boxes represent broad averaging windows calculated by combining individual measurements from all eastern equatorial Pacific sites. Thereby, *x*-axis extent of the boxes represents the stratigraphic range from which measurements are pooled and the *y*-axis extent represents 68% and 95% confidence intervals considering both analytical and calibration uncertainty. Boxes are numbered 1 to 4 as shown in the bar above Panel (a). Panels (b) and (c) show benthic foraminiferal $\delta^{18}O$ and $\delta^{13}C$ data, respectively, from Sites U1334 (Taylor et al., 2023b), 1218 (Coxall & Wilson, 2011; Coxall et al., 2005), and U1333 (this study) for the samples measured during Δ_{47} analysis (horizontal bars as in a) and the independently generated high-resolution $\delta^{18}O$ and $\delta^{13}C$ record, respectively, from Site U1334 (gray; Taylor et al., 2023b). The Eocene-Oligocene Transition is defined following Hutchinson et al. (2021) (refer to Figure S1 in Supporting Information S1).

combined foraminiferal calibration of Meinicke et al. (2020), updated to the I-CDES scale (Meinicke et al., 2021). The impact of calibration choice on calculated absolute temperatures is minor (Figure S2 in Supporting Information S1). We report sample errors of our Δ_{47}-derived BWTs as 68% and 95% confidence intervals (Fernandez et al., 2017), combining both analytical and calibration uncertainty using Monte Carlo simulation (n = 5,000). Uncertainty in the ETF is incorporated into mean Δ_{47} values by ensuring that the measurement of samples combined within each averaging group (individual temperatures and box groups) were spread across long time intervals (at least several months) (Daëron, 2021). Our BWTs and $\delta^{18}O_b$ values are substituted into the (*Cibicidoides spp.*-specific) paleotemperature equation of Marchitto et al. (2014) to calculate $\delta^{18}O_{sw}$. To avoid introducing additional uncertainty into $\delta^{18}O_{sw}$ calculations from inter-species $\delta^{18}O$ offset corrections, we use independently generated $\delta^{18}O_b$ values from Sites U1334 (*Cibicidoides grimsdalei*; Taylor et al., 2023b) and 1218 (*Cibicidoides* spp.; Coxall & Wilson, 2011; Coxall et al., 2005), which were measured on the same samples used for Δ_{47} analysis.

3. Results and Discussion

3.1. Deep-Sea Temperature Change in the Eastern Equatorial Pacific

To track BWT change across the EOT, we produced Δ_{47}-derived BWT records from three neighboring sites in the deep EEP (Figure 1). Our most detailed record comes from Site U1334 (Figure 2, circles), which, in the lead-up to the onset of Antarctic glaciation, benefits from the highest sedimentation rates, highest carbonate contents, and best benthic foraminiferal preservation of the EEP sites (Edgar et al., 2013; Taylor et al., 2023b). We also present Δ_{47}-derived BWT records from neighboring sites 1218 (Figure 2, squares) and U1333 (Figure 2, triangles). We use these data to test the reproducibility of our BWT record from Site U1334. Despite the taphonomical gradient between sites (Edgar et al., 2013), reconstructed absolute temperatures from Sites U1334, 1218, and U1333 are all within error of one another and the records take the same overall form (Figure 2a and Figure S3 in Supporting Information S1). This result further suggests that there is only a minor influence of diagenetic overprinting on benthic foraminiferal Δ_{47} values in typical deep ocean settings (Leutert et al., 2019). The specific effect of dissolution remains to be explicitly tested, but our new records suggest that its effect on benthic foraminiferal Δ_{47} values may be minimal. Crucially for our study, the congruence in reconstructed temperatures among sites and detailed inter-site correlations (Westerhold et al., 2012, 2014) allow us to combine all EEP Δ_{47} measurements to capture temperature changes across the main phases of the EOT with greater precision. Guided by our $\delta^{13}C_b$ and $\delta^{18}O_b$ data series (Figures 2b and 2c) we define four broad averaging windows within which we combine measurements from all three EEP sites: 35.02 to 34.33 Ma (Figure 2a, box 4), 34.01 to 33.78 Ma (Figure 2a, box 3), 33.70 to 33.63 Ma (Figure 2a, box 2), and 33.60 to 33.01 Ma (Figure 2a, box 1). Using these broad averaging windows, we define baseline BWTs for the late Eocene (pre-EOT) and early Oligocene (post-EOT) and constrain BWT change across (a) "Step 1," (b) the EOIS, and (c) the long-term net change across the EOT.

Using this approach, we find that average BWTs in the EEP range from 6.5 ± 0.9°C to 11.1 ± 0.6°C during our study interval (uncertainty reported at 68% confidence intervals combining both analytical and calibration uncertainty; Figure 2a, boxes). These temperatures are appreciably warmer than modern seafloor temperatures in the deep EEP (~1.5°C; Locarnini et al., 2010). Our reconstructed BWT range is, however, compatible with

25724525, 2023, 8, Downloaded from https://agupubs.onlinelibrary.wiley.com/doi/10.1029/2023PA004650 by University Of Southampton, Wiley Online Library on [09/10/2023]. See the Terms and Conditions (https://onlinelibrary.wiley.com/terms-and-conditions) on Wiley Online Library for rules of use; OA articles are governed by the applicable Creative Commons License

10.1029/2023PA004650

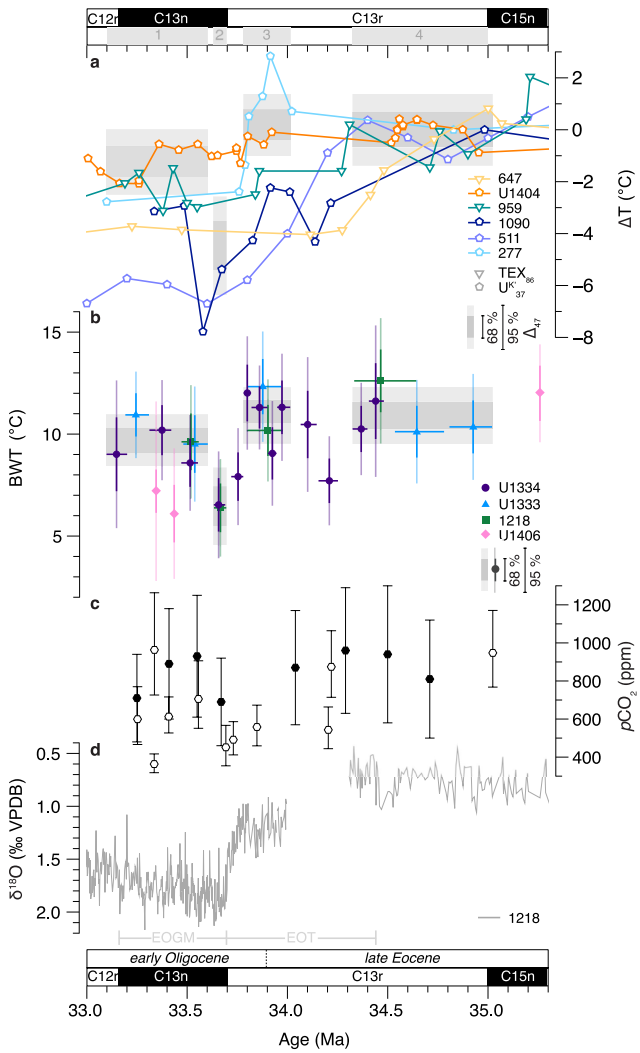

Figure 3. Comparison of CO_2 and temperature reconstructions across the Eocene-Oligocene Transition. Panel (a) compares relative temperature changes in the surface ocean compared to our record of bottom-water temperature (BWT) in the eastern equatorial Pacific (EEP). Surface ocean temperature records (open symbols) are shown from Sites 647 in the southern Labrador Sea (Sliwińska et al., 2023), U1404 in the North Atlantic (Liu et al., 2018), 511 in the South Atlantic (Liu et al., 2009), 959 in the equatorial Atlantic (Cramwinckel et al., 2018), 1090 in the Atlantic sector of the Southern Ocean (Liu et al., 2009), and 277 in the Pacific sector of the Southern Ocean (Liu et al., 2009). $U^{K'}_{37}$ records are shown as pentagons and TEX_{86} records are shown as inverted triangles. Temperature change is calculated relative to a late Eocene baseline defined as the average of temperatures between 35.5 and 34.5 Ma. Gray boxes show relative deep ocean temperature change calculated for the broad averaging windows shown in Figure 2. Panel (b) shows Δ_{47}-derived BWTs (closed symbols) for Sites U1334 (circles), 1218 (squares), and U1333 (triangles) as in Figure 2, in addition to BWTs for Site U1406 (diamonds; Meckler et al., 2022). Panel (c) shows atmospheric carbon dioxide concentration (pCO_2) reconstructions derived from boron isotopes (filled hexagons; Pearson et al., 2009) and alkenones (open hexagons; Pagani et al., 2011, recalculated by Zhang et al., 2020). Panel (d) shows the benthic foraminiferal $\delta^{18}O$ record for Site 1218 (Coxall & Wilson, 2011; Coxall et al., 2005) for reference. All EEP records are shown on the common astronomically calibrated age model of Westerhold et al. (2014). Published surface ocean temperature records are updated to GTS2012.

contemporaneous surface ocean warmth (~12°C to ~25°C; Figure S4 in Supporting Information S1) in the high-latitude Southern Hemisphere (e.g., Houben et al., 2019; Liu et al., 2009; Pagani et al., 2011; Plancq et al., 2014), which is a potential source region of deep-waters in the EEP during the late Eocene and early Oligocene (McKinley et al., 2019; Thomas et al., 2008). These warm high-latitude Southern Hemisphere surface ocean temperatures are corroborated by clumped isotope records (Figure S5 in Supporting Information S1; Douglas et al., 2014; Petersen & Schrag, 2015). Our warm deep-sea temperatures are also comparable to those associated with other intervals of Antarctic ice sheet expansion, such as the middle Miocene (~5°C to ~12°C; Lear et al., 2015; Leutert et al., 2021; Modestou et al., 2020). The warm BWTs that we reconstruct for the EOT therefore add to a growing body of evidence pointing toward the capacity for dynamic behavior of the early Antarctic ice sheets under warmer conditions than today.

We identify three broad features in the evolution of BWTs in the EEP at the EOT. First, we reconstruct no net cooling across "Step 1" (Figure 2a, boxes 4 to 3). We note that at Site U1334, where the EOT is most stratigraphically expanded, there is no evidence to support the suggestion that "Step 1" is marked by a rapid $\delta^{18}O_b$ increase (Taylor et al., 2023b). Instead, $\delta^{18}O_b$ values increase gradually from ~1.2 to ~1.7‰ over ~300 kyrs between ~34.0 Ma and ~33.7 Ma (Taylor et al., 2023b). According to our new data, this gradual $\delta^{18}O_b$ increase is not associated with deep ocean cooling (Figure 2). The latest Eocene is instead characterized by an interval of sustained warmth during which BWTs average 11.1 ± 0.6°C in the EEP (Figure 2a, box 3), similar to the average BWT of 10.9 ± 0.7°C prior to "Step 1." Second, we reconstruct an abrupt major cooling at "Step-2" (EOIS) whereby BWTs in the EEP cooled by 4.7 ± 0.9°C (Figure 2a, boxes 3 to 2) to an average of 6.5 ± 0.9°C (Figure 2a, box 2). These coldest early Oligocene BWTs are statistically distinct from those immediately prior to the EOIS, and during the pre- and post-EOT intervals (Figure S6 in Supporting Information S1). This finding represents the first robust and direct evidence of deep-sea cooling across the EOIS and strongly suggests that the $\delta^{18}O_b$ "overshoot" at the base of the EOGM (Liu et al., 2004; Zachos et al., 1996) contains a substantial component of deep-sea cooling in the EEP (Figure 2). Third, the major cooling across the EOIS is short-lived. Within 300 kyrs, BWTs in the EEP rebound to temperatures of 9.7 ± 0.6°C (Figure 2a, box 1), close to those of the late Eocene (10.9 ± 0.7°C; Figure 2a, box 4). A similar structure of change is seen in $\delta^{18}O_b$, however, unlike BWTs, $\delta^{18}O_b$ values do not fully return to pre-EOIS values within the same timeframe (Figure 2). This suggests a progressively diminishing role for temperature in driving high $\delta^{18}O_b$ values during the EOGM.

3.2. Ocean Temperature Change at the Eocene-Oligocene Transition

The lack of cooling that we document in our records for "Step 1" (Figures 3a and 3b, boxes 4 to 3) is not a unique result. Sustained warmth into the latest Eocene, immediately prior to the main phase of Antarctic ice sheet expansion is also seen in SST records from the mid-latitudes of the South Pacific Ocean at Sites 277 (Figure 3a) (Liu et al., 2009; Pagani et al., 2011) and 1172 (Houben et al., 2019). At these latitudes in the Atlantic Ocean, however, there is a marked cooling demonstrating strong spatial heterogeneity in the temperature response to global change (Figure 3a). More detailed records from both the surface and deep ocean during this interval are needed to determine the spatial extent of this sustained latest Eocene warmth and assess its impact on preconditioning Antarctica for large-scale glaciation across the EOIS.

25724525, 2023, 8, Downloaded from https://agupubs.onlinelibrary.wiley.com/doi/10.1029/2023PA004650 by University Of Southampton, Wiley Online Library on [09/10/2023]. See the Terms and Conditions (https://onlinelibrary.wiley.com/terms-and-conditions) on Wiley Online Library for rules of use; OA articles are governed by the applicable Creative Commons License

The magnitude of cooling that we reconstruct in the deep EEP across the EOIS (4.7 ± 0.9°C; Figures 3a and 3b, box 3 to 2) is consistent with the cooling observed in SSTs in the mid-latitude southern hemisphere across the EOT and with associated model estimates of global deep ocean cooling (3–5°C) (Figure 3a) (Liu et al., 2009). This abrupt cooling signal in our records is correlative with the rapid high-amplitude over-deepening in the CCD (Taylor et al., 2023b, Figure S3 in Supporting Information S1) which likely explains why a contemporaneous cooling is not documented by deep-sea benthic foraminiferal Mg/Ca records (Figure S7 in Supporting Information S1), including the one from Site 1218 (Lear et al., 2004, 2010).

Some (but not all) other temperature records suggest an, at least partial, rebound in temperatures following cooling at the onset of large-scale Antarctic glaciation. A partial temperature recovery during the early Oligocene is observed in terrestrial temperature records (e.g., Amoo et al., 2021; Colwyn & Hren, 2019; Lauretano et al., 2021), in records from low latitude continental shelf sites (Katz et al., 2008; Lear et al., 2008) and in many other SST records (Figure 3a) (Bohaty et al., 2012; Liu et al., 2009, 2018). The coarse resolution of many of these records prevents an assessment of the rate of this rebound in the surface ocean, but warm SSTs, akin to those of the middle-to-late Eocene, are seen for most of the Oligocene (see O'Brien et al., 2020 for a recent compilation). Taken together, these data sets, alongside our new record of deep ocean temperature change in the EEP, suggest a partial recovery in temperatures during the early Oligocene following the inception of Antarctic ice sheets (Figure 3a, boxes 2 to 1). A similar structure is suggested in low-resolution reconstructions of atmospheric carbon dioxide concentrations (Figure 3c) (Pagani et al., 2011; Pearson et al., 2009 recalculated by Zhang et al., 2020). Some records from the mid-latitudes in the southern hemisphere are the main exception to this, with surface ocean temperatures records from Sites 277 and 511 (Figure 3; Houben et al., 2019; Liu et al., 2009) suggesting a long-term cooling across the EOT. The same is not, however, true at Site 1090 (Figure 3; Liu et al., 2009) or in the Atlantic-sector Southern Ocean Site 689 (Bohaty et al., 2012) and Indian-sector Southern Ocean Sites 738, 744, and 748 (Bohaty et al., 2012), suggesting a strong degree of heterogeneity in the surface ocean response in the high Southern latitudes. Further work is needed to investigate the heterogeneity in these records, especially in the Southern Ocean.

Given the spatial heterogeneity and temporal variability in surface ocean SSTs during the EOT (Figure 3a and Figure S4 in Supporting Information S1), we might expect the response of the deep ocean to have been spatially heterogenous. A comparison with the few available Δ_{47}-derived BWTs from the North Atlantic Ocean supports spatial heterogeneity in deep ocean temperatures across the EOT. While our EEP BWTs across the EOT are comparable with BWTs from the North Atlantic Ocean for the middle to late Eocene, they are warmer than those documented for the early Oligocene North Atlantic Ocean (by ∼2°C to ∼5°C; Meckler et al., 2022; Figure 3b, box 1). Further work is needed to better characterize the temperature histories of the different deep ocean basins at a resolution sufficient to capture the different phases of the EOT.

3.3. Late Eocene to Early Oligocene Seawater $\delta^{18}O$ and Antarctic Ice Sheets

To calculate $\delta^{18}O_{sw}$ at our EEP study sites, we combine our Δ_{47}-derived BWTs and $\delta^{18}O_b$ values. The $\delta^{18}O_{sw}$ values are set by a combination of global continental ice volume and local deep-sea salinity. The absolute $\delta^{18}O_{sw}$ values we reconstruct for the EEP range from 0.2 ± 0.2 to 0.8 ± 0.1‰, and are, therefore, consistently much higher than the value for an "ice-free world" ($\delta^{18}O_{sw}$ ∼ −0.9 to −1.2‰) estimated by oxygen isotope mass balance (Cramer et al., 2011; Shackleton & Kennett, 1975; Zachos et al., 2001) (Figure 4d). The high $\delta^{18}O_{sw}$ values that we calculate are not dependent on our choice of Δ_{47}-temperature calibration (Figure S2 in Supporting Information S1). Higher-than-expected $\delta^{18}O_{sw}$ values are also not unique to our setting, time interval, or paleothermometer. Similarly high deep-sea $\delta^{18}O_{sw}$ values have been reconstructed for much of the Paleogene (Meckler et al., 2022) and into the middle Miocene (e.g., Lear et al., 2015; Leutert et al., 2021; Modestou et al., 2020), and calculated using both Δ_{47} and Mg/Ca-derived BWTs.

The $\delta^{18}O_{sw}$ values we reconstruct are too high to be explained solely by continental ice volume, even if we account for the greater sub-aerially exposed land area available for ice accumulation on Antarctica at the EOT (Paxman et al., 2019; Wilson et al., 2012). This is especially true when we consider the following: (a) the isotopic composition of the initial ice sheet was likely less isotopically depleted than today (Coxall et al., 2005; Edgar et al., 2007), requiring an even larger ice volume to account for our reconstructed high $\delta^{18}O_{sw}$ values, (b) contemporaneous Southern Hemisphere high latitude warmth (Bohaty et al., 2012; Houben et al., 2019; Liu et al., 2009; Petersen & Schrag, 2015) and vegetated Antarctic coastal regions (Francis et al., 2008), and (c) large-scale

25724525, 2023, 8, Downloaded from https://agupubs.onlinelibrary.wiley.com/doi/10.1029/2023PA004650 by University Of Southampton, Wiley Online Library on [09/10/2023]. See the Terms and Conditions (https://onlinelibrary.wiley.com/terms-and-conditions) on Wiley Online Library for rules of use; OA articles are governed by the applicable Creative Commons License

10.1029/2023PA004650

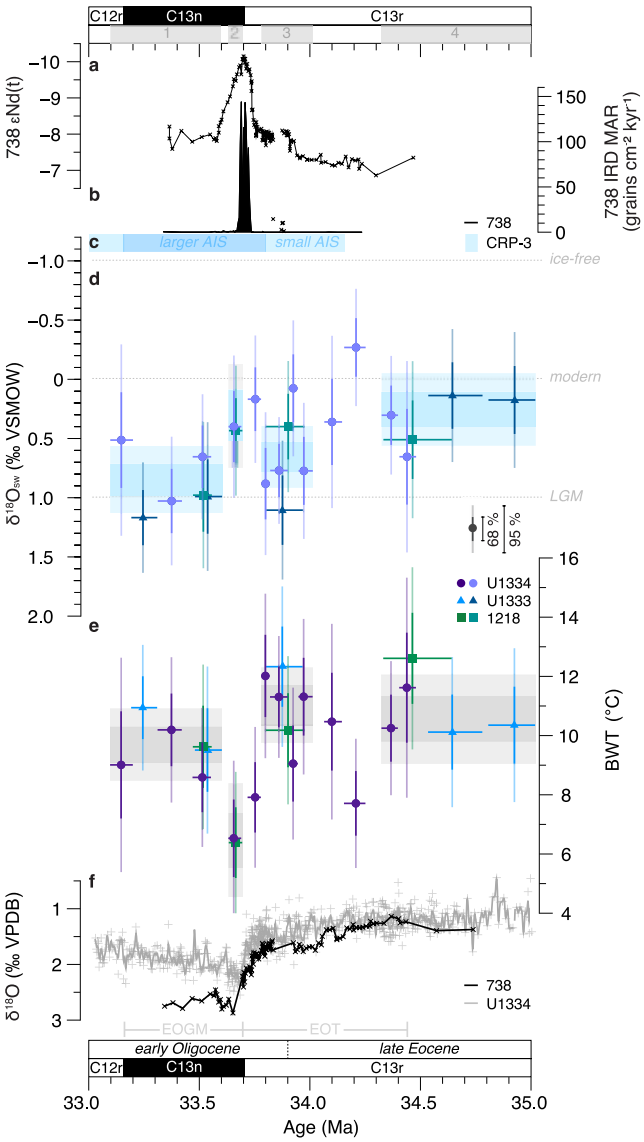

Figure 4. Seawater $\delta^{18}O$ reconstructions from the eastern equatorial Pacific. Panels (a) and (b) show fish tooth neodymium isotopes and IRD accumulation rate records, respectively, from Site 738 (Kerguelen Plateau; Scher et al., 2011) interpreted to represent the onset of large-scale Antarctic glaciation. Panel (c) indicates the inferred size of the Antarctic ice sheet based on analysis of sedimentary cycles in the CRP-3 drill core in the Ross Sea (Galeotti et al., 2016). Panel (d) shows calculated $\delta^{18}O_{sw}$ values for Sites U1334 (circles), 1218 (squares), and U1333 (triangles). Horizontal bars represent the stratigraphic range from which measurements are pooled, and *y*-axis error bars represent propagated temperature errors as 68% and 95% confidence intervals. Panel (e) shows Δ_{47}-derived BWTs for Sites U1334 (circles), 1218 (squares), and U1333 (triangles) as in Figure 2. Boxes represent average $\delta^{18}O_{sw}$ (d) and BWTs (e) calculated by combining individual measurements from all EEP sites. Bar *x*-axis extent represents the stratigraphic range from which measurements are pooled and the bar *y*-axis extent represents 68% and 95% confidence intervals considering both analytical and calibration uncertainty. Panel (f) shows benthic foraminiferal $\delta^{18}O$ records from Site U1334 (gray; Taylor et al., 2023b) and Site 738 (black; Scher et al., 2011).

Northern Hemisphere ice sheets were not established at the EOT (Spray et al., 2019). Other environmental factors, therefore, likely contribute to the high $\delta^{18}O_{sw}$ values that we report. These could be related to non-thermal influences on $\delta^{18}O_b$, such as physiological effects during foraminiferal calcite precipitation which are not accounted for in the $\delta^{18}O$-temperature calibration (in this study we use Marchitto et al., 2014). Another possible explanation for higher-than-expected calculated $\delta^{18}O_{sw}$ values could be an influence of lower seawater pH (Meckler et al., 2022; Zeebe, 2001). Lower ocean pH has been shown to increase planktic foraminiferal $\delta^{18}O$ values (Spero et al., 1997; Uchikawa & Zeeve, 2010), while the influence on Δ_{47} values is negligible by comparison (Guo, 2020; Tang et al., 2014; Tripati et al., 2015). Although the relationship between deep ocean pH and $\delta^{18}O_b$ values remains less clear (Marchitto et al., 2014), correcting $\delta^{18}O_b$ values for the long-term deep ocean pH trend would bring calculated overall $\delta^{18}O_{sw}$ values closer to those predicted using sea level reconstructions (Cramer et al., 2011; Meckler et al., 2022). Alternatively, $\delta^{18}O_{sw}$ values could be higher due to storage of isotopically light water in other continental reservoirs, such as groundwater, which would increase baseline $\delta^{18}O_{sw}$ values. This has been suggested as a possible mechanism to explain Cretaceous sea level variability in the absence of ice sheets (Sames et al., 2020; Wendler et al., 2016). An isolated, and fresher, Arctic Ocean basin (Onodera et al., 2008; Straume et al., 2020; Waddell & Moore, 2008) may also act as a reservoir of isotopically light water. Greater interaction between seawater and oceanic crust could also elevate long-term $\delta^{18}O_{sw}$ values (Jaffrés et al., 2007; Wallmann, 2001). Finally, elevated $\delta^{18}O_{sw}$ values could indicate that a more saline bottom-water mass is bathing the deep EEP, as has been suggested to explain comparably high $\delta^{18}O_{sw}$ values during the middle Miocene (Lear et al., 2015; Modestou et al., 2020). A saltier bottom-water mass in the deep Pacific would need to be compensated for by a comparatively fresher water mass elsewhere. Different gateway and basin configurations may have led to a less globally connected deep ocean circulation, relative to the modern ocean, which presents the potential for greater heterogeneity in the properties of contemporaneous deep-water masses. Future work should test for this possibility by generating comparable records from other ocean basins.

Although factors other than ice volume are probably needed to explain the high $\delta^{18}O_{sw}$ values, and water mass changes could in principle also contribute to relative changes in $\delta^{18}O_{sw}$, expansion of continental ice volume was likely the dominant driver of long-term $\delta^{18}O_{sw}$ change from the late Eocene to early Oligocene, given the Antarctic-proximal evidence for glaciation at the EOT (Ehrmann & Mackensen, 1992; Galeotti et al., 2016; Hambrey et al., 1991; Passchier et al., 2017; Scher et al., 2011; Zachos et al., 1992). We reconstruct an overall net increase in deep EEP $\delta^{18}O_{sw}$ of 0.6 ± 0.2‰ from the late Eocene to early Oligocene (Figure 4d, boxes 4 to 1). This result is comparable to surface ocean estimates of the overall $\delta^{18}O_{sw}$ change across the EOT from the Indian Ocean (Lear et al., 2008), Southern Ocean (Bohaty et al., 2012; Petersen & Schrag, 2015) and southeast Atlantic Ocean (Peck et al., 2010). The agreement between ocean basins supports the suggestion that the overall $\delta^{18}O_{sw}$ increase across the EOT represents a global $\delta^{18}O_{sw}$ increase, most likely related to continental ice volume. An increase of ~0.6‰ is consistent with the growth of an Antarctic ice sheet 70%–110% as large as today, and a ~40–60 m fall in global mean sea level (Bohaty et al., 2012; Edgar et al., 2007; Lear et al., 2008; Liu et al., 2009). Our new data suggest that an Antarctic ice sheet of at least this size was sustained into the early Oligocene and bottom-water in the deep EEP at the EOT was

25724525, 2023, 8, Downloaded from https://agupubs.onlinelibrary.wiley.com/doi/10.1029/2023PA004650 by University Of Southampton, Wiley Online Library on [09/10/2023]. See the Terms and Conditions (https://onlinelibrary.wiley.com/terms-and-conditions) on Wiley Online Library for rules of use; OA articles are governed by the applicable Creative Commons License

likely sourced from the Southern Ocean, with convection sites proximal to Antarctica (McKinley et al., 2019; Thomas et al., 2008), implying a close connection between temperatures in the deep EEP and the Antarctic ice sheet. However, temperatures in the deep Pacific rebounded to levels close to those of the late Eocene by approximately 33.6 Ma (Figure 4). The apparent continued presence of a large-scale Antarctic ice sheet during the early Oligocene in the context of rebounding ocean temperatures in the deep EEP (Figures 4d and 4e) and many other locations in the surface ocean (Section 3.2) therefore suggests a partial decoupling between the early Antarctic ice sheet and ocean temperatures (Figures 3 and 4). This partial decoupling implies that the main control on the mass balance of the early Antarctic ice sheet on this timescale may have been the competition between the stabilizing effects of ice sheet elevation and profile (Paxman et al., 2019; Pollard & DeConto, 2005) and top-down melting through atmospheric forcing. The likely absence of ice shelves under warmer, higher pCO_2 conditions (Gasson et al., 2016) would have limited the role of ocean-driven melting and may help to explain the apparent decoupling between the early Antarctic ice sheet and ocean temperatures in the early Oligocene. Furthermore, the impact of ice volume changes on deep ocean temperatures has been suggested to be largely related to ice sheet extent, rather than volume, suggesting that an inland ice sheet growing in height may have had a minimal impact on BWTs (Bradshaw et al., 2021).

3.4. Deep-Sea Cooling Prior to the Onset of Large-Scale Antarctic Glaciation

Decoupling between ocean temperature and apparent ice sheet growth is also observed in some of the smaller-scale details of our record. First, our data from Site U1334 record a transient cooling of 3.9 ± 1.9°C in the latest Eocene between ~34.35 and ~34.1 Ma, which is unaccompanied by change in $\delta^{18}O_b$ (Figure 2). In our record, BWTs reach a minimum of 7.7 ± 1.1°C by ~34.21 Ma, closely associated with the end-Eocene nCIE (Figure 2) and CCD shoaling event (Figure S3 in Supporting Information S1; Taylor et al., 2023b), suggesting close coupling of this cooling signal to a perturbation of the carbon cycle. Second, our data from Site U1334 suggest that the main phase of deep ocean cooling in the EEP began about 100 kyrs before the main phase of EOT $\delta^{18}O_b$ increase (Figure 2). We can rule out aliasing through either inadvertent analysis of reworked foraminifera specimens or by our averaging approach, because the individual $\delta^{13}C_b$ and $\delta^{18}O_b$ values acquired in concert with the lower Δ_{47} temperatures are consistent with the base of the EOIS (Figure 2). Because these two prominent cooling signals are unaccompanied by major increases in $\delta^{18}O_b$, they are associated with calculated decreases in $\delta^{18}O_{sw}$ that are superimposed upon the overall long-term pattern (a $\delta^{18}O_{sw}$ increase). While decreases in $\delta^{18}O_{sw}$ records post-EOT typically signify deglaciation events, that process is unlikely to offer an explanation here because of robust sedimentological and geochemical evidence for ice sheet advance across the EOIS (Figure 4; e.g., Galeotti et al., 2016; Passchier et al., 2017; Scher et al., 2011). An alternative explanation for the decreases in $\delta^{18}O_{sw}$ seen in our record is that they reflect either a shift between two different water masses bathing the deep EEP (i.e., a warmer and saltier water mass vs. a cooler and fresher water mass) or a temporary change in the properties (freshening) of the dominant bottom water mass. Assuming a modern regional $\delta^{18}O_{sw}$-salinity relationship for the deep Pacific Ocean (LeGrande & Schmidt, 2006), these negative $\delta^{18}O_{sw}$ excursions would require a change in salinity in the deep EEP of up to 1.5 to 2 psu. The current lack of constraints on deep-sea hydrography during the EOT does not allow us to differentiate between these two scenarios but we suggest that the shorter-term variability in deep EEP $\delta^{18}O_{sw}$ could be traceable to a highly dynamic and expanding early Antarctic ice sheet exerting influence on ocean circulation configuration and vigor (Goldner et al., 2014).

4. Conclusions

Clumped isotope thermometry provides a way to deconvolve deep-sea $\delta^{18}O_b$ records. Our benthic foraminiferal clumped isotope records from three sites in the deep EEP provide new independent constraints on the evolution of deep-sea temperatures and $\delta^{18}O_{sw}$ across the EOT. The congruence in our records across three EEP sites, despite their varying water depths, attests to the robustness of our reconstructed temperatures and allows us to combine Δ_{47} measurements to document the magnitude of deep-sea temperature change during the EOT with greater confidence. We identify four main features of the EOT deep-sea temperature record in the EEP: (a) late Eocene to early Oligocene temperatures in the deep EEP were ~5 to ~10°C warmer than seafloor temperatures there today, (b) no net temperature change is documented associated with EOT $\delta^{18}O_b$ "Step 1," (c) major cooling (~4.7 ± 0.9°C) is documented for the main phase of $\delta^{18}O_b$ increase at the EOT (EOIS, i.e., $\delta^{18}O_b$ "Step 2"), and (d) this "Step 2" cooling event was short-lived, lasting only ~200 kyrs, temperatures rebounded to near pre-EOT

25724525, 2023, 8, Downloaded from https://agupubs.onlinelibrary.wiley.com/doi/10.1029/2023PA004650 by University Of Southampton, Wiley Online Library on [09/10/2023]. See the Terms and Conditions (https://onlinelibrary.wiley.com/terms-and-conditions) on Wiley Online Library for rules of use; OA articles are governed by the applicable Creative Commons License

levels by 33.6 Ma. Our records, therefore, suggest that there was no discernible overall change in BWTs in the EEP between climate states both with and without a large Antarctic ice sheet. Further work is needed to improve data coverage and depeen our mechanistic understanding of the EOT. Short-term episodes of deep-sea cooling during various phases of the EOT may have played an important role in preconditioning the Earth system for large-scale Antarctic ice sheet expansion.

Our calculated record of seawater $\delta^{18}O$ change suggests the continued presence of a large-scale Antarctic ice sheet in the early Oligocene while deep-sea temperatures returned to those akin to the late Eocene. This interpretation relies on the assumption that the observed long-term increase in $\delta^{18}O_{sw}$ is entirely a global signal related to Antarctic ice sheet expansion. If confirmed by comparable records from other ocean basins, the partial decoupling between ocean temperature and ice volume suggests that the self-stabilizing effects associated with the growth of the early Antarctic ice sheet were strong enough to withstand the effect of subsequent warming as indicated in our ocean temperature record.

Data Availability Statement

This research used samples and data provided by the International Ocean Discovery Program (IODP). Temperature data are available on Pangaea at Taylor et al. (2023c). Benthic foraminiferal stable isotope records for Sites U1334 and 1218 are available at Taylor et al. (2023a), and Coxall et al. (2005) and Coxall and Wilson (2011), respectively.

Acknowledgments
This work was funded by the European Research Council (ERC) under the European Union's Horizon 2020 research and innovation programme (grant agreement no. 638467; awarded to ANM) and the Norwegian Research Council (project number 314371; awarded to ANM). This work was also supported by Natural Environment Research Council (NERC) Grants NE/K014137/1 and NE/K008390/1 to PAW, NE/K006800/1 to SMB and PAW, a Royal Society Wolfson Merit Award to PAW, and a NERC SPITIFRE Doctoral Training Program Studentship (NE/L002531/1) awarded to VET and supervised by PAW and SMB. The authors thank Lubna Al-Saadi, Nil Irvali, Enver Alagoz, and Eirik Galaasen for technical support during sample preparation and clumped isotope analyses at the University of Bergen, Megan Wilding and Bastian Hambach for technical support at the University of Southampton, Phil Rumford and colleagues at the IODP Gulf Coast Core Repository for assistance with sampling, and Alvaro Fernandez and Sevasti Modestou for thoughtful discussions. We thank the Editor, Associate Editor and Reviewers for their constructive and thorough reviews which improved this manuscript. For the purposes of open access, the author has applied a CC BY public copyright license to any Author Accepted Manuscript version arising from this submission.

References

Amoo, M., Salzmann, U., Pound, M., Thompson, N., & Bijl, P. (2021). Eocene to Oligocene vegetation and climate in the Tasmanian Gateway region controlled by changes in ocean currents and *p*CO2. In *Climate of the past discussions* (pp. 1–35). https://doi.org/10.5194/cp-2021-131

Bernasconi, S. M., Daëron, M., Bergmann, K. D., Bonifacie, M., Meckler, A. N., Affek, H. P., et al. (2021). InterCarb: A community effort to improve interlaboratory standardization of the carbonate clumped isotope thermometer using carbonate standards. *Geochemistry, Geophysics, Geosystems*, *22*(5), 1–25. https://doi.org/10.1029/2020GC009588

Bernasconi, S. M., Hu, B., Wacker, U., Fiebig, J., Breitenbach, S. F. M., & Rutz, T. (2013). Background effects on Faraday collectors in gas-source mass spectrometry and implications for clumped isotope measurements. *Rapid Communications in Mass Spectrometry*, *27*(5), 603–612. https://doi.org/10.1002/rcm.6490

Bernasconi, S. M., Müller, I. A., Bergmann, K. D., Breitenbach, S. F. M., Fernandez, A., Hodell, D. A., et al. (2018). Reducing uncertainties in carbonate clumped isotope analysis through consistent carbonate-based standardization. *Geochemistry, Geophysics, Geosystems*, *19*(9), 2895–2914. https://doi.org/10.1029/2017GC007385

Billups, K., & Schrag, D. P. (2003). Application of benthic foraminiferal Mg/Ca ratios to questions of Cenozoic climate change. *Earth and Planetary Science Letters*, *209*(1–2), 181–195. https://doi.org/10.1016/S0012-821X(03)00067-0

Bohaty, S. M., Zachos, J. C., & Delaney, M. L. (2012). Foraminiferal Mg/Ca evidence for Southern Ocean cooling across the Eocene-Oligocene transition. *Earth and Planetary Science Letters*, *317–318*, 251–261. https://doi.org/10.1016/j.epsl.2011.11.037

Bradshaw, C. D., Langebroak, P. M., Lear, C. H., Lunt, D. J., Coxall, H. K., Sosdian, S. M., & de Boer, A. M. (2021). Hydrological impact of Middle Miocene Antarctic ice-free areas coupled to deep ocean temperatures. *Nature Geoscience*, *14*(6), 429–436. https://doi.org/10.1038/s41561-021-00745-w

Brand, W. A., Assonov, S. S., & Coplen, T. B. (2010). Correction for the ^{17}O interference in $\delta^{13}C$ measurements when analyzing CO_2 with stable isotope mass spectrometry (IUPAC Technical Report). *Pure and Applied Chemistry*, *82*(8), 1719–1733. https://doi.org/10.1351/PAC-REP-09-01-05

Colwyn, D. A., & Hren, M. T. (2019). An abrupt decrease in Southern Hemisphere terrestrial temperature during the Eocene–Oligocene transition. *Earth and Planetary Science Letters*, *512*, 227–235. https://doi.org/10.1016/j.epsl.2019.01.052

Coxall, H. K., Huck, C. E., Huber, M., Lear, C. H., Legarda-Lisarri, A., O'Regan, M., et al. (2018). Export of nutrient rich northern component water preceded early Oligocene Antarctic glaciation/704/106/413/704/829/704/106/2738 article. *Nature Geoscience*, *11*(3), 190–196. https://doi.org/10.1038/s41561-018-0069-9

Coxall, H. K., & Wilson, P. A. (2011). Early Oligocene glaciation and productivity in the eastern equatorial Pacific: Insights into global carbon cycling. *Paleoceanography*, *26*(2), 1–18. https://doi.org/10.1029/2010PA002021

Coxall, H. K., Wilson, P. A., Pälike, H., Lear, C. H., & Backman, J. (2005). Rapid stepwise onset of Antarctic glaciation and deeper calcite compensation in the Pacific Ocean. *Nature*, *433*(7021), 53–57. https://doi.org/10.1038/nature03135

Cramer, B. S., Miller, K. G., Barrett, P. J., & Wright, J. D. (2011). Late Cretaceous-Neogene trends in deep ocean temperature and continental ice volume: Reconciling records of benthic foraminiferal geochemistry ($\delta^{18}O$ and Mg/Ca) with sea level history. *Journal of Geophysical Research*, *116*(12), 1–23. https://doi.org/10.1029/2011JC007255

Cramwinckel, M. J., Huber, M., Kocken, I. J., Agnini, C., Bijl, P. K., Bohaty, S. M., et al. (2018). Synchronous tropical and polar temperature evolution in the Eocene letter. *Nature*, *559*(7714), 382–386. https://doi.org/10.1038/s41586-018-0272-2

Daëron, M. (2021). Full propagation of analytical uncertainties in Δ_{47} measurements. *Geochemistry, Geophysics, Geosystems*, *22*(5), 1–19. https://doi.org/10.1029/2020GC009592

Daëron, M., Blamart, D., Peral, M., & Affek, H. P. (2016). Absolute isotopic abundance ratios and the accuracy of Δ_{47} measurements. *Chemical Geology*, *442*, 83–96. https://doi.org/10.1016/j.chemgeo.2016.08.014

DeConto, R. M., & Pollard, D. (2003). Rapid Cenozoic glaciation of Antarctica induced by declining atmospheric CO_2. *Nature*, *421*(6920), 245–249. https://doi.org/10.1038/nature01290

25724525, 2023, 8, Downloaded from https://agupubs.onlinelibrary.wiley.com/doi/10.1029/2023PA004650 by University Of Southampton, Wiley Online Library on [09/10/2023]. See the Terms and Conditions (https://onlinelibrary.wiley.com/terms-and-conditions) on Wiley Online Library for rules of use; OA articles are governed by the applicable Creative Commons License

Douglas, P. M. J., Affek, H. P., Ivany, L. C., Houben, A. J. P., Sijp, W. P., Sluijs, A., et al. (2014). Pronounced zonal heterogeneity in Eocene southern high-latitude sea surface temperatures. *Proceedings of the National Academy of Sciences of the United States of America*, *111*(18), 6582–6587. https://doi.org/10.1073/pnas.1321441111

Eagle, R. A., Eiler, J. M., Tripati, A. K., Ries, J. B., Freitas, P. S., Hiebenthal, C., et al. (2013). The influence of temperature and seawater carbonate saturation state on ^{13}C-^{18}O bond ordering in bivalve mollusks. *Biogeosciences*, *10*(7), 4591–4606. https://doi.org/10.5194/bg-10-4591-2013

Edgar, K. M., Pälike, H., & Wilson, P. A. (2013). Testing the impact of diagenesis on the $\delta^{18}O$ and $\delta^{13}C$ of benthic foraminiferal calcite from a sediment burial depth transect in the equatorial Pacific. *Paleoceanography*, *28*(3), 468–480. https://doi.org/10.1002/palo.20045

Edgar, K. M., Wilson, P. A., Sexton, P. F., & Suganuma, Y. (2007). No extreme bipolar glaciation during the main Eocene calcite compensation shift. *Nature*, *448*(7156), 908–911. https://doi.org/10.1038/nature06053

Ehrmann, W. U., & Mackensen, A. (1992). Sedimentological evidence for the formation of an East Antarctic ice sheet in Eocene/Oligocene time. *Palaeogeography, Palaeoclimatology, Palaeoecology*, *93*(1–2), 85–112. https://doi.org/10.1016/0031-0182(92)90185-8

Eiler, J. M. (2011). Paleoclimate reconstruction using carbonate clumped isotope thermometry. *Quaternary Science Reviews*, *30*(25–26), 3575–3588. https://doi.org/10.1016/j.quascirev.2011.09.001

Elderfield, H., Yu, J., Anand, P., Kiefer, T., & Nyland, B. (2006). Calibrations for benthic foraminiferal Mg/Ca paleothermometry and the carbonate ion hypothesis. *Earth and Planetary Science Letters*, *250*(3–4), 633–649. https://doi.org/10.1016/j.epsl.2006.07.041

Evans, D., Sagoo, N., Renema, W., Cotton, L. J., Müller, W., Todd, J. A., et al. (2018). Eocene greenhouse climate revealed by coupled clumped isotope-Mg/Ca thermometry. *Proceedings of the National Academy of Sciences of the United States of America*, *115*(6), 1174–1179. https://doi.org/10.1073/pnas.1714744115

Fernandez, A., Müller, I. A., Rodríguez-Sanz, L., van Dijk, J., Looser, N., & Bernasconi, S. M. (2017). A reassessment of the precision of carbonate clumped isotope measurements: Implications for calibrations and paleoclimate reconstructions. *Geochemistry, Geophysics, Geosystems*, *18*(12), 4375–4386. https://doi.org/10.1002/2017GC007106

Francis, J. E., Marenssi, S., Levy, R., Hambrey, M., Thorn, V. C., Mohr, B., et al. (2008). Chapter 8 from greenhouse to icehouse—The Eocene/Oligocene in Antarctica. In *Developments in Earth and environmental sciences* (Vol. 8). https://doi.org/10.1016/S1571-9197(08)00008-6

Galeotti, S., DeConto, R., Naish, T., Stocchi, P., Florindo, F., Pagani, M., et al. (2016). Antarctic Ice Sheet variability across the Eocene-Oligocene boundary climate transition. *Science*, *352*(6281), 76–80. https://doi.org/10.1126/science.aab0669

Gasson, E., DeConto, R. M., Pollard, D., & Levy, R. H. (2016). Dynamic Antarctic ice sheet during the early to mid-Miocene. *Proceedings of the National Academy of Sciences of the United States of America*, *113*(13), 3459–3464. https://doi.org/10.1073/pnas.1516130113

Ghosh, P., Adkins, J., Affek, H., Balta, B., Guo, W., Schauble, E. A., et al. (2006). ^{13}C-^{18}O bonds in carbonate minerals: A new kind of paleothermometer. *Geochimica et Cosmochimica Acta*, *70*(6), 1439–1456. https://doi.org/10.1016/j.gca.2005.11.014

Goldner, A., Herold, N., & Huber, M. (2014). Antarctic glaciation caused ocean circulation changes at the Eocene-Oligocene transition. *Nature*, *511*(7511), 574–577. https://doi.org/10.1038/nature13597

Grauel, A. L., Schmid, T. W., Hu, B., Bergami, C., Capotondi, L., Zhou, L., & Bernasconi, S. M. (2013). Calibration and application of the "clumped isotope" thermometer to foraminifera for high-resolution climate reconstructions. *Geochimica et Cosmochimica Acta*, *108*, 125–140. https://doi.org/10.1016/j.gca.2012.12.049

Guo, W. (2020). Kinetic clumped isotope fractionation in the DIC-H_2O-CO_2 system: Patterns, controls, and implications. *Geochimica et Cosmochimica Acta*, *258*, 230–257. https://doi.org/10.1016/j.gca.2019.07.055

Hambrey, M. J., Ehrmann, W. U., & Larsen, B. (1991). Cenozoic glacial record of the Prydz Bay continental shelf, East Antarctica. In *Proceeding of scientific results, ODP, Leg 119, Kerguelen Plateau-Prydz Bay, September, 77–132*. https://doi.org/10.2973/odp.proc.sr.119.200.1991

Hill, P. S., Tripati, A. K., & Schauble, E. A. (2014). Theoretical constraints on the effects of pH, salinity, and temperature on clumped isotope signatures of dissolved inorganic carbon species and precipitating carbonate minerals. *Geochimica et Cosmochimica Acta*, *125*, 610–652. https://doi.org/10.1016/j.gca.2013.06.018

Houben, A. J. P., Bijl, P. K., Sluijs, A., Schouten, S., & Brinkhuis, H. (2019). Late Eocene Southern Ocean cooling and invigoration of circulation preconditioned Antarctica for full-scale glaciation. *Geochemistry, Geophysics, Geosystems*, *20*(5), 2214–2234. https://doi.org/10.1029/2019GC008182

Houben, A. J. P., van Mourik, C. A., Montanari, A., Coccioni, R., & Brinkhuis, H. (2012). The Eocene-Oligocene transition: Changes in sea level, temperature or both? *Palaeogeography, Palaeoclimatology, Palaeoecology*, *335–336*, 75–83. https://doi.org/10.1016/j.palaeo.2011.04.008

Hu, B., Radke, J., Schlüter, H. J., Heine, F. T., Zhou, L., & Bernasconi, S. M. (2014). A modified procedure for gas-source isotope ratio mass spectrometry: The long-integration dual-inlet (LIDI) methodology and implications for clumped isotope measurements. *Rapid Communications in Mass Spectrometry*, *28*(13), 1413–1425. https://doi.org/10.1002/rcm.6909

Hutchinson, D. K., Coxall, H. K., Lunt, D. J., Steinthorsdottir, M., De Boer, A. M., Baatsen, M., et al. (2021). The Eocene-Oligocene transition: A review of marine and terrestrial proxy data, models and model-data comparisons. *Climate of the Past*, *17*(1), 269–315. https://doi.org/10.5194/cp-17-269-2021

Jaffrés, J. B. D., Shields, G. A., & Wallmann, K. (2007). The oxygen isotope evolution of seawater: A critical review of a long-standing controversy and an improved geological water cycle model for the past 3.4 billion years. *Earth-Science Reviews*, *83*(1–2), 83–122. https://doi.org/10.1016/j.earscirev.2007.04.002

John, C. M., & Bowen, D. (2016). Community software for challenging isotope analysis: First applications of 'Easotope' to clumped isotopes. *Rapid Communications in Mass Spectrometry*, *30*(21), 2285–2300. https://doi.org/10.1002/rcm.7720

Katz, M. E., Miller, K. G., Wright, J. D., Wade, B. S., Browning, J. V., Cramer, B. S., & Rosenthal, Y. (2008). Stepwise transition from the Eocene greenhouse to the Oligocene icehouse. *Nature Geoscience*, *1*(5), 329–334. https://doi.org/10.1038/ngeo179

Kennett, J. P., & Shackleton, N. J. (1976). Oxygen isotopic evidence for the development of the psychrosphere 38 Myr ago. *Nature*, *260*(6), 513–515. https://doi.org/10.1038/260513a0

Kocken, I. J., Müller, I. A., & Ziegler, M. (2019). Optimizing the use of carbonate standards to minimize uncertainties in clumped isotope data. *Geochemistry, Geophysics, Geosystems*, *20*(11), 5565–5577. https://doi.org/10.1029/2019GC008545

Koppers, A. A. P., Morgan, J. P., Morgan, J. W., & Staudigel, H. (2001). Testing the fixed hotspot hypothesis using $^{40}Ar/^{39}Ar$ age progressions along seamount trails. *Earth and Planetary Science Letters*, *185*(3–4), 237–252. https://doi.org/10.1016/S0012-821X(00)00387-3

Langton, S. J., Rabideaux, N. M., Borrelli, C., & Katz, M. E. (2016). Southeastern Atlantic deep-water evolution during the late-middle Eocene to earliest Oligocene (Ocean Drilling Program site 1263 and Deep Sea Drilling project site 366). *Geosphere*, *12*(3), 1032–1047. https://doi.org/10.1120/GES01268.1

Lauretano, V., Kennedy-Asser, A. T., Korasidis, V. A., Wallace, M. W., Valdes, P. J., Lunt, D. J., et al. (2021). Eocene to Oligocene terrestrial Southern Hemisphere cooling caused by declining pCO_2. *Nature Geoscience*, *14*(9), 659–664. https://doi.org/10.1038/s41561-021-00788-z

Lear, C. H., Bailey, T. R., Pearson, P. N., Coxall, H. K., & Rosenthal, Y. (2008). Cooling and ice growth across the Eocene-Oligocene transition. *Geology*, *36*(3), 251–254. https://doi.org/10.1130/G24584A.1

25724525, 2023, 8, Downloaded from https://agupubs.onlinelibrary.wiley.com/doi/10.1029/2023PA004650 by University Of Southampton, Wiley Online Library on [09/10/2023]. See the Terms and Conditions (https://onlinelibrary.wiley.com/terms-and-conditions) on Wiley Online Library for rules of use; OA articles are governed by the applicable Creative Commons License

Lear, C. H., Coxall, H. K., Foster, G. L., Lunt, D. J., Mawbey, E. M., Rosenthal, Y., et al. (2015). Neogene ice volume and ocean temperatures: Insights from infaunal foraminiferal Mg/Ca paleothermometry. *Paleoceanography*, *30*(11), 1437–1454. https://doi.org/10.1002/2015PA002833. Received

Lear, C. H., Elderfield, H., & Wilson, P. A. (2000). Cenozoic deep-sea temperatures and global ice volumes from Mg/Ca in benthic foraminiferal calcite. *Science*, *287*(5451), 269–272. https://doi.org/10.1126/science.287.5451.269

Lear, C. H., Mawbey, E. M., & Rosenthal, Y. (2010). Cenozoic benthic foraminiferal Mg/Ca and Li/Ca records: Toward unlocking temperatures and saturation states. *Paleoceanography*, *25*(4), 1–11. https://doi.org/10.1029/2009PA001880

Lear, C. H., Rosenthal, Y., Coxall, H. K., & Wilson, P. A. (2004). Late Eocene to early Miocene ice sheet dynamics and the global carbon cycle. *Paleoceanography*, *19*(4), 1–11. https://doi.org/10.1029/2004PA001039

LeGrande, A. N., & Schmidt, G. A. (2006). Global gridded data set of the oxygen isotopic composition in seawater. *Geophysical Research Letters*, *33*(12), L12604. https://doi.org/10.1029/2006GL026011

Leutert, T. J., Auderset, A., Martínez-García, A., Modestou, S., & Meckler, A. N. (2020). Coupled Southern Ocean cooling and Antarctic ice sheet expansion during the middle Miocene. *Nature Geoscience*, *13*(9), 634–639. https://doi.org/10.1038/s415161-020-0623-0

Leutert, T. J., Modestou, S., Bernasconi, S. M., & Meckler, A. N. (2021). Southern ocean bottom-water cooling and ice sheet expansion during the middle Miocene climate transition. *Climate of the Past*, *17*(5), 2255–2271. https://doi.org/10.5194/cp-17-2255-2021

Leutert, T. J., Sexton, P. F., Tripati, A., Piasecki, A., Ho, S. L., & Meckler, A. N. (2019). Sensitivity of clumped isotope temperatures in fossil benthic and planktic foraminifera to diagenetic alteration. *Geochimica et Cosmochimica Acta*, *257*, 354–372. https://doi.org/10.1016/j.gca.2019.05.005

Liu, Z., He, Y., Jiang, Y., Wang, H., Liu, W., Bohaty, S. M., & Wilson, P. A. (2018). Transient temperature asymmetry between hemispheres in the palaeogene Atlantic Ocean. *Nature Geoscience*, *11*(9), 656–660. https://doi.org/10.1038/s41561-018-0182-9

Liu, Z., Pagani, M., Zinniker, D., Deconto, R., Huber, M., Brinkhuis, H., et al. (2009). Global cooling during the Eocene-Oligocene climate transition. *Science*, *323*(5918), 1187–1190. https://doi.org/10.1126/science.1166368

Liu, Z., Tuo, S., Zhao, Q., Cheng, X., & Huang, W. (2004). Deep-water earliest Oligocene glacial maximum (EOGM) in South Atlantic. *Chinese Science Bulletin*, *49*(20), 2190–2197. https://doi.org/10.1360/04wd0228

Locarnini, R. A., Mishonov, A. V., Antonov, J. I., Boyer, T. P., Garcia, H. E., Baranova, K. O., et al. (2010). World Ocean Atlas 2009 NOAA Atlas NESDIS 69 WORLD OCEAN ATLAS 2009 volume 1: Temperature. In S. Levitus (Ed.), *NOAA Atlas NESDIS 68, Issue December 2015*. U.S. Government Printing Office.

Lyle, M., Barron, J., Bralower, T. J., Huber, M., Lyle, A. O., Ravelo, A. C., et al. (2008). Pacific Ocean and cenozoic evolution of climate. *Reviews of Geophysics*, *46*(2), 1–47. https://doi.org/10.1029/2005RG000190

Lyle, M., Wilson, P. A., & Janecek, T. R. (2002). Leg 199 summary. In *Proceedings of the Ocean Drilling Program, 199 initial reports* (Vol. 199). https://doi.org/10.2973/odp.proc.ir.199.101.2002

Marchitto, T. M., Curry, W. B., Lynch-Stieglitz, J., Bryan, S. P., Cobb, K. M., & Lund, D. C. (2014). Improved oxygen isotope temperature calibrations for cosmopolitan benthic foraminifera. *Geochimica et Cosmochimica Acta*, *130*, 1–11. https://doi.org/10.1016/j.gca.2013.12.034

McKinley, C. C., Thomas, D. J., LeVay, L. J., & Rolewicz, Z. (2019). Nd isotopic structure of the Pacific Ocean 40–10 Ma, and evidence for the reorganization of deep North Pacific Ocean circulation between 36 and 25 Ma. *Earth and Planetary Science Letters*, *521*, 139–149. https://doi.org/10.1016/j.epsl.2019.06.009

Meckler, A. N., Sexton, P. F., Piasecki, A. M., Leutert, T. J., Marquardt, J., Ziegler, M., et al. (2022). Cenozoic evolution of deep ocean temperature from clumped isotope thermometry. *Science*, *377*(6601), 86–90. https://doi.org/10.1126/science.abk0604

Meckler, A. N., Ziegler, M., Millán, M. I., Breitenbach, S. F. M., & Bernasconi, S. M. (2014). Long-term performance of the Kiel carbonate device with a new correction scheme for clumped isotope measurements. *Rapid Communications in Mass Spectrometry*, *28*(15), 1705–1715. https://doi.org/10.1002/rcm.6949

Meinicke, N., Ho, S. L., Hannisdal, B., Nürnberg, D., Tripati, A., Schiebel, R., & Meckler, A. N. (2020). A robust calibration of the clumped isotopes to temperature relationship for foraminifers. *Geochimica et Cosmochimica Acta*, *270*, 160–183. https://doi.org/10.1016/j.gca.2019.11.022

Meinicke, N., Reimi, M. A., Ravelo, A. C., & Meckler, A. N. (2021). Coupled Mg/Ca and clumped isotope measurements indicate lack of substantial mixed layer cooling in the Western pacific warm pool during the last ∼5 million years. *Paleoceanography and Paleoclimatology*, *36*(8), e2020PA004115. https://doi.org/10.1029/2020PA004115

Miller, K. G., Browning, J. V., Aubry, M. P., Wade, B. S., Katz, M. E., Kulpecz, A. A., & Wright, J. D. (2008). Eocene–Oligocene global climate and sea-level change changes: St. Stephens Quarry, Alabama. *Geological Society of America Bulletin*, *120*(1–2), 34–53. https://doi.org/10.1130/B26105.1

Miller, K. G., Browning, J. V., John Schmelz, W., Kopp, R. E., Mountain, G. S., & Wright, J. D. (2020). Cenozoic sea-level and cryospheric evolution from deep-sea geochemical and continental margin records. *Science Advances*, *6*(20), eaaz1346. https://doi.org/10.1126/sciadv.aaz1346

Modestou, S. E., Leutert, T. J., Fernandez, A., Lear, C. H., & Meckler, A. N. (2020). Warm middle Miocene Indian Ocean bottom water temperatures: Comparison of clumped isotope and Mg/Ca-based estimates. *Paleoceanography and Paleoclimatology*, *35*(11), e2020PA003927. https://doi.org/10.1029/2020PA003927

Müller, I. A., Fernandez, A., Radke, J., van Dijk, J., Bowen, D., Schwieters, J., & Bernasconi, S. M. (2017). Carbonate clumped isotope analyses with the long-integration dual-inlet (LIDI) workflow: Scratching at the lower sample weight boundaries. *Rapid Communications in Mass Spectrometry*, *31*(12), 1057–1066. https://doi.org/10.1002/rcm.7878

Norris, R. D., Wilson, P. A., Blum, P., Fehr, A., Agnini, C., Bornemann, A., et al. (2014). Expedition 342 summary. In R. D. Norris, P. A. Wilson, P. Blum, & the Expedition 342 Scientists (Eds.), *Proceedings of the Ocean Drilling Program* (Vol. 342). https://doi.org/10.2204/iodp.proc.342.101.2014

O'Brien, C. L., Huber, M., Thomas, E., Pagani, M., Super, J. R., Elder, L. E., & Hull, P. M. (2020). The enigma of Oligocene climate and global surface temperature evolution. *Proceedings of the National Academy of Sciences of the United States of America*, *117*(41), 25302–25309. https://doi.org/10.1073/pnas.2003914117

Onodera, J., Takahashi, K., & Jordan, R. W. (2008). Eocene silicoflagellate and ebridian paleoceanography in the central Arctic Ocean. *Paleoceanography*, *23*(1), PA1S15. https://doi.org/10.1029/2007PA001474

Pagani, M., Huber, M., Liu, Z., Bohaty, S. M., Henderiks, J., Sijp, W., et al. (2011). The role of carbon dioxide during the onset of Antarctic glaciation. *Science*, *334*(6060), 1261–1264. https://doi.org/10.1126/science.1203909

Pälike, H., Lyle, M., Nishi, H., Raffi, I., Gamage, K., & Klaus, A. (2010). Expedition 320/321 summary. In *Proceedings of the Integrated Ocean Drilling Program* (Vol. 320). https://doi.org/10.2204/iodp.proc.320321.101.2010

Pälike, H., Lyle, M. W., Nishi, H., Raffi, I., Ridgwell, A., Gamage, K., et al. (2012). A Cenozoic record of the equatorial Pacific carbonate compensation depth. *Nature*, *488*(7413), 609–614. https://doi.org/10.1038/nature11360

25724525, 2023, 8, Downloaded from https://agupubs.onlinelibrary.wiley.com/doi/10.1029/2023PA004650 by University Of Southampton, Wiley Online Library on [09/10/2023]. See the Terms and Conditions (https://onlinelibrary.wiley.com/terms-and-conditions) on Wiley Online Library for rules of use; OA articles are governed by the applicable Creative Commons License

Passchier, S., Ciarletta, D. J., Miriagos, T. E., Bijl, P. K., & Bohaty, S. M. (2017). An Antarctic stratigraphic record of stepwise ice growth through the Eocene-Oligocene transition. *Bulletin of the Geological Society of America*, *129*(3–4), 318–330. https://doi.org/10.1130/B31482.1

Paxman, G. J. G., Jamieson, S. S. R., Hochmuth, K., Gohl, K., Bentley, M. J., Leitchenkov, G., & Ferraccioli, F. (2019). Reconstructions of Antarctic topography since the Eocene–Oligocene boundary. *Palaeogeography, Palaeoclimatology, Palaeoecology*, *535*(May), 109346. https://doi.org/10.1016/j.palaeo.2019.109346

Pearson, P. N., Foster, G. L., & Wade, B. S. (2009). Atmospheric carbon dioxide through the Eocene-Oligocene climate transition. *Nature*, *461*(7267), 1110–1113. https://doi.org/10.1038/nature08447

Pearson, P. N., McMillan, I. K., Wade, B. S., Jones, T. D., Coxall, H. K., Bown, P. R., & Lear, C. H. (2008). Extinction and environmental change across the Eocene-Oligocene boundary in Tanzania. *Geology*, *36*(2), 179–182. https://doi.org/10.1130/G24308A.1

Peck, V. L., Yu, J., Kender, S., & Riesselman, C. R. (2010). Shifting ocean carbonate chemistry during the Eocene-Oligocene climate transition: Implications for deep-ocean Mg/Ca paleothermometry. *Paleoceanography*, *25*(4), 1–9. https://doi.org/10.1029/2009PA001906

Pekar, S. F., Christie-Blick, N., Kominz, M. A., & Miller, K. G. (2002). Calibration between eustatic estimates from backstripping and oxygen isotopic records for the Oligocene. *Geology*, *30*(10), 903–906. https://doi.org/10.1130/0091-7613(2002)030<0903:cbeefb>2.0.co;2

Peral, M., Daëron, M., Blamart, D., Bassinot, F., Dewilde, F., Smialkowski, N., et al. (2018). Updated calibration of the clumped isotope thermometer in planktonic and benthic foraminifera. *Geochimica et Cosmochimica Acta*, *239*, 1–16. https://doi.org/10.1016/j.gca.2018.07.016

Petersen, S. V., & Schrag, D. P. (2015). Antarctic ice growth before and after the Eocene-Oligocene transition: New estimates from clumped isotope paleothermometry. *Paleoceanography*, *30*(10), 1305–1317. https://doi.org/10.1002/2014PA002769

Piasecki, A., Bernasconi, S. M., Grauel, A. L., Hannisdal, B., Ho, S. L., Leutert, T. J., et al. (2019). Application of clumped isotope thermometry to benthic foraminifera. *Geochemistry, Geophysics, Geosystems*, *20*(4), 2082–2090. https://doi.org/10.1029/2018GC007961

Plancq, J., Mattioli, E., Pittet, B., Simon, L., & Grossi, V. (2014). Productivity and sea-surface temperature changes recorded during the late Eocene-early Oligocene at DSDP site 511 (South Atlantic). *Palaeogeography, Palaeoclimatology, Palaeoecology*, *407*, 34–44. https://doi.org/10.1016/j.palaeo.2014.04.016

Pollard, D., & DeConto, R. M. (2005). Hysteresis in cenozoic Antarctic ice-sheet variations. *Global and Planetary Change*, *45*(1–3), 9–21. https://doi.org/10.1016/j.gloplacha.2004.09.011

Pusz, A. E., Thunell, R. C., & Miller, K. G. (2011). Deep water temperature, carbonate ion, and ice volume changes across the Eocene-Oligocene climate transition. *Paleoceanography*, *26*(2), 1–15. https://doi.org/10.1029/2010PA001950

Rodríguez-Sanz, L., Bernasconi, S. M., Marino, G., Heslop, D., Müller, I. A., Fernandez, A., et al. (2017). Penultimate deglacial warming across the Mediterranean Sea revealed by clumped isotopes in foraminifera. *Scientific Reports*, *7*(1), 1–11. https://doi.org/10.1038/s41598-017-16528-6

Sames, B., Wagreich, M., Conrad, C. P., & Iqbal, S. (2020). Aquifer-eustasy as the main driver of short-term sea-level fluctuations during cretaceous hothouse climate phases. *Geological Society Special Publication*, *498*(1), 9–38. https://doi.org/10.1144/SP498-2019-105

Savin, S. M. (1977). The history of the Earth's surface temperature during the past 100 million years. *Annual Review of Earth and Planetary Sciences*, *5*(1), 319–355. https://doi.org/10.1146/annurev.ea.05.050177.001535

Savin, S. M., Douglas, R. G., & Stehli, F. G. (1975). Tertiary marine paleotemperatures. *Geological Society of America Bulletin*, *86*(11), 1499–1510. https://doi.org/10.1130/0016-7606(1975)86<1499:tmp>2.0.co;2

Schauble, E. A., Ghosh, P., & Eiler, J. M. (2006). Preferential formation of ^{13}C-^{18}O bonds in carbonate minerals, estimated using first-principles lattice dynamics. *Geochimica et Cosmochimica Acta*, *70*(10), 2510–2529. https://doi.org/10.1016/j.gca.2006.02.011

Scher, H. D., Bohaty, S. M., Zachos, J. C., & Delaney, M. L. (2011). Two-stepping into the icehouse: East Antarctic weathering during progressive ice-sheet expansion at the Eocene-Oligocene transition. *Geology*, *39*(4), 383–386. https://doi.org/10.1130/G31726.1

Schmid, T. W., & Bernasconi, S. M. (2010). An automated method for 'clumped-isotope' measurements on small carbonate samples. *Rapid Communications in Mass Spectrometry*, *24*(14), 1955–1963. https://doi.org/10.1002/rcm.4598

Shackleton, N. J., & Kennett, J. P. (1975). Paleotemperature history of the cenozoic and the initiation of Antarctic glaciation: Oxygen and carbon isotope analyses in DSDP sites 277, 279, and 281. In *Initial report of the deep sea drilling project 29* (pp. 743–755).

Śliwińska, K. K., Coxall, H. K., Hutchinson, D. K., Liebrand, D., Schouten, S., & de Boer, A. M. (2023). Sea surface temperature evolution of the North Atlantic Ocean across the Eocene-Oligocene transition. *Climate of the Past*, *19*(1), 123–140. https://doi.org/10.5194/cp-19-123-2023

Śliwińska, K. K., Thomsen, E., Schouten, S., Schoon, P. L., & Heilmann-Clausen, C. (2019). Climate- and gateway-driven cooling of late Eocene to earliest Oligocene sea surface temperatures in the North sea basin. *Scientific Reports*, *9*(1), 1–11. https://doi.org/10.1038/s41598-019-41013-7

Spero, H. J., Bijma, J., Lea, D. W., & Meis, B. E. (1997). Effect of seawater carbonate concentration on foraminiferal carbon and oxygen isotopes. *Nature*, *390*(6659), 497–500. https://doi.org/10.1038/37333

Spray, J. F., Bohaty, S. M., Davies, A., Bailey, I., Romans, B. W., Cooper, M. J., et al. (2019). North Atlantic evidence for a unipolar icehouse climate state at the Eocene-Oligocene transition. *Paleoceanography and Paleoclimatology*, *34*(7), 1124–1138. https://doi.org/10.1029/2019PA003563

Straume, E. O., Gaina, C., Medvedev, S., & Nisancioglu, K. H. (2020). Global cenozoic paleobathymetry with a focus on the Northern Hemisphere Oceanic gateways. *Gondwana Research*, *86*, 126–143. https://doi.org/10.1016/j.gr.2020.05.011

Tang, J., Dietzel, M., Fernandez, A., Tripati, A. K., & Rosenheim, B. E. (2014). Evaluation of kinetic effects on clumped isotope fractionation (δ_{47}) during inorganic calcite precipitation. *Geochimica et Cosmochimica Acta*, *134*, 120–136. https://doi.org/10.1016/j.gca.2014.03.005

Taylor, V. E., Westerhold, T., Bohaty, S. M., Backman, J., Dunkley Jones, T., Edgar, K. M., et al. (2023a). Benthic foraminiferal and bulk sediment stable isotope records, and carbonate content records from the eastern equatorial Pacific, and a reconstruction of the calcite compensation depth across the EOT [Dataset]. Pangaea. https://doi.org/10.1594/PANGAEA.956848

Taylor, V. E., Westerhold, T., Bohaty, S. M., Backman, J., Dunkley Jones, T., Edgar, K. M., et al. (2023b). Transient shoaling, over-deepening and settling of the calcite compensation depth at the Eocene-Oligocene transition. *Paleoceanography and Paleoclimatology*, *38*(6), e2022PA004493. https://doi.org/10.1029/2022PA004493

Taylor, V. E., Wilson, P. A., Bohaty, S. M., & Meckler, A. N. (2023c). Deep ocean temperatures in the eastern equatorial Pacific Ocean at the Eocene-Oligocene transition [Dataset]. Pangaea. https://doi.org/10.1594/PANGAEA.961094

Thomas, D. J., Lyle, M., Moore, T. C., & Rea, D. K. (2008). Paleogene deep water mass composition of the tropical Pacific and implications for thermohaline circulation in a greenhouse world. *Geochemistry, Geophysics, Geosystems*, *9*(2), 1–13. https://doi.org/10.1029/2007GC001748

Tremblin, M., Hermoso, M., & Minoletti, F. (2016). Equatorial heat accumulation as a long-term trigger of permanent Antarctic ice sheets during the Cenozoic. *Proceedings of the National Academy of Sciences of the United States of America*, *113*(42), 11782–11787. https://doi.org/10.1073/pnas.1608100113

Tripati, A. K., Eagle, R. A., Thiagarajan, N., Gagnon, A. C., Bauch, H., Halloran, P. R., & Eiler, J. M. (2010). ^{13}C-^{18}O isotope signatures and "clumped isotope" thermometry in foraminifera and coccoliths. *Geochimica et Cosmochimica Acta*, *74*(20), 5697–5717. https://doi.org/10.1016/j.gca.2010.07.006

25724525, 2023, 8, Downloaded from https://agupubs.onlinelibrary.wiley.com/doi/10.1029/2023PA004650 by University Of Southampton, Wiley Online Library on [09/10/2023]. See the Terms and Conditions (https://onlinelibrary.wiley.com/terms-and-conditions) on Wiley Online Library for rules of use; OA articles are governed by the applicable Creative Commons License

Tripati, A. K., Hill, P. S., Eagle, R. A., Mosenfelder, J. L., Tang, J., Schauble, E. A., et al. (2015). Beyond temperature: Clumped isotope signatures in dissolved inorganic carbon species and the influence of solution chemistry on carbonate mineral composition. *Geochimica et Cosmochimica Acta*, *166*, 344–371. https://doi.org/10.1016/j.gca.2015.06.021

Uchikawa, J., & Zeeve, R. E. (2010). Examining possible effects of seawater pH decline on foraminiferal stable isotopes during the Paleocene-Eocene Thermal Maximum. *Paleoceanograhy*, *25*(2), PA2216. https://doi.org/10.1029/2009pa001864

Waddell, L. M., & Moore, T. C. (2008). Salinity of the Eocene Arctic Ocean from oxygen isotope analysis of fish bone carbonate. *Paleoceanography*, *23*(1), PA1S12. https://doi.org/10.1029/2007PA001451

Wade, B. S., Houben, A. J. P., Quaijtaal, W., Schouten, S., Rosenthal, Y., Miller, K. G., et al. (2012). Multiproxy record of abrupt sea-surface cooling across the Eocene-Oligocene transition in the Gulf of Mexico. *Geology*, *40*(2), 159–162. https://doi.org/10.1130/G32577.1

Wallmann, K. (2001). The geological water cycle and the evolution of marine $\delta^{18}O$ values. *Geochimica et Cosmochimica Acta*, *65*(15), 2469–2485. https://doi.org/10.1016/S0016-7037(01)00603-2

Watkins, J. M., & Hunt, J. D. (2015). A process-based model for non-equilibrium clumped isotope effects in carbonates. *Earth and Planetary Science Letters*, *432*, 152–165. https://doi.org/10.1016/j.epsl.2015.09.042

Wendler, J. E., Wendler, I., Vogt, C., & Kuss, J. (2016). Link between cyclic eustatic sea-level change and continental weathering: Evidence for aquifer-eustasy in the Cretaceous. *Palaeogeography, Palaeoclimatology, Palaeoecology*, *441*, 430–437. https://doi.org/10.1016/j.palaeo.2015.08.014

Westerhold, T., Marwan, N., Drury, A. J., Liebrand, D., Agnini, C., Anagnostou, E., et al. (2020). An astronomically dated record of Earth's climate and its predictability over the last 66 million years. *Science*, *369*(6509), 1383–1388. https://doi.org/10.1126/SCIENCE.ABA6853

Westerhold, T., Röhl, U., Pälike, H., Wilkens, R., Wilson, P. A., & Acton, G. (2014). Orbitally tuned timescale and astronomical forcing in the middle Eocene to early Oligocene. *Climate of the Past*, *10*(3), 955–973. https://doi.org/10.5194/cp-10-955-2014

Westerhold, T., Röhl, U., Wilkens, R., Pälike, H., Lyle, M., Jones, T. D., et al. (2012). Revised composite depth scales and integration of IODP Sites U1331-U1334 and ODP Sites 1218–1220. In H. Pälike, M. Lyle, H. Nishi, I. Raffi, K. Gamage, A. Klaus, et al. (Eds.), *Proceedings of the Ocean Drilling Program: Vol. 320/321*. https://doi.org/10.2204/iodp.proc.320321.201.2012

Wilson, D. S., Jamieson, S. S. R., Barrett, P. J., Leitchenkov, G., Gohl, K., & Larter, R. D. (2012). Antarctic topography at the Eocene-Oligocene boundary. *Palaeogeography, Palaeoclimatology, Palaeoecology*, *335–336*, 24–34. https://doi.org/10.1016/j.palaeo.2011.05.028

Yu, J., & Elderfield, H. (2008). Mg/Ca in the benthic foraminifera Cibicidoides wuellerstorfi and Cibicidoides mundulus: Temperature versus carbonate ion saturation. *Earth and Planetary Science Letters*, *276*(1–2), 129–139. https://doi.org/10.1016/j.epsl.2008.09.015

Zachos, J. C., Breza, J. R., & Wise, S. W. (1992). Early Oligocene ice-sheet expansion on Antarctica: Stable isotope and sedimentological evidence from Kerguelen plateau, southern Indian Ocean. *Geology*, *20*(6), 569–573. https://doi.org/10.1130/0091-7613(1992)020<0569:EOISEO>2.3.CO;2

Zachos, J. C., Pagani, M., Sloan, L., Thomas, E., & Billups, K. (2001). Trends, rhythms, and Aberrations in global climate 65 Ma to present. *Science*, *292*(5517), 686–693. https://doi.org/10.1126/science.1059412

Zachos, J. C., Quinn, T. M., & Salamy, K. A. (1996). High-resolution (104 years) deep-sea foraminiferal stable isotope records of the Eocene-Oligocene climate transition. *Paleoceanography*, *11*(3), 251–266. https://doi.org/10.1029/96PA00571

Zeebe, R. E. (2001). Seawater pH and isotopic paleotemperatures of Cretaceous oceans. *Palaeogeography, Palaeoclimatology, Palaeoecology*, *170*(1–2), 49–57. https://doi.org/10.1016/S0031-0182(01)00226-7

Zhang, Y. G., Henderiks, J., & Liu, X. (2020). Refining the alkenone-pCO_2 method II: Towards resolving the physiological parameter b. *Geochimica et Cosmochimica Acta*, *281*, 118–134. https://doi.org/10.1016/j.gca.2020.05.002

References From the Supporting Information

Laskar, J., Fienga, A., Gastineau, M., & Manche, H. (2011). La2010: A new orbital solution for the long-term motion of the Earth. *Astronomy & Astrophysics*, *532*, A89. https://doi.org/10.1051/0004-6361/201116836

Laskar, J., Robutel, P., Joutel, F., Gastineau, M., Correia, A. C. M., & Levrard, B. (2004). A long-term numerical solution for the insolation quantities of the Earth. *Astronomy & Astrophysics*, *428*(1), 261–285. https://doi.org/10.1051/0004-6361:20041335

25724525, 2023, 8, Downloaded from https://agupubs.onlinelibrary.wiley.com/doi/10.1029/2023PA004650 by University Of Southampton, Wiley Online Library on [09/10/2023]. See the Terms and Conditions (https://onlinelibrary.wiley.com/terms-and-conditions) on Wiley Online Library for rules of use; OA articles are governed by the applicable Creative Commons License